

# A nanostructured genosensor for the early diagnosis of systemic arterial hypertension

Thalita Rolim · Juliana Cancino · Valtencir Zucolotto

© Springer Science+Business Media New York 2015

**Abstract** The rapid progress of nanomedicine, especially in areas related to medical imaging and diagnostics, has motivated the development of new nanomaterials that can be combined with biological materials for specific medical applications. One such area of research involves the detection of specific DNA sequences for the early diagnosis of genetic diseases, using nanoparticles-containing genosensors. Typical genosensors devices are based on the use of sensing electrodes – biorecognition platforms - containing immobilized capture DNA probes capable of hybridizing with specific target DNA sequences. In this paper we show that upon an appropriate design of the biorecognition platform, efficient sandwich-type genosensors based upon DNA-AuNPs nanocomplexes can be efficiently applied to the detection of a Systemic Arterial Hypertension (SAH) polymorphism located in intron 16 of the Angiotensin-converter enzyme (ACE) gene. Since SAH is intimately related to heart diseases, especially blood hypertension, its early detection is of great biomedical interest. The biorecognition platforms were assembled using mixed self-assembled monolayers (SAM<sub>mix</sub>), which provided the immobilization of organized architectures with molecular control. Detection of the DNA target sequence at concentrations down to 1 nM was carried out using electrochemical impedance spectroscopy (EIS). We show that the use of EIS combined with specific nanobiocomplexes represents an efficient

method for the unambiguous detection of complementary DNA hybridization for preventative nanomedicine applications.

**Keywords** Genosensor · Systemic arterial hypertension · Oligonucleotides · Nanocomplexes · Electrochemical impedance spectroscopy

## 1 Introduction

The use of biomolecules-functionalized nanomaterials, or nanobioconjugates, has attracted great attention in medical areas as efficient materials for diagnosis and therapy (Davis, Zuckerman et al. 2010; Heidel and Davis 2011). These nanobioconjugates have been used, for example, as biosensors and for drug delivery (Sinha, Kim et al. 2006; Bonanni and del Valle 2010; Dykman and Khlebtsov 2012), contrast in imaging diagnostics (Hellebust and Richards-Kortum 2012), protein immobilization (Lee, Park et al. 2002), markers for target cell and cancer treatment (Kennedy, Bickford et al. 2011), and recognizing and extracting cancerous cells (Garnica-Garza 2009; Geng, Song et al. 2011), in which both the nanomaterial and the biomolecule can mimic the required biological conditions (Sinha, Kim et al. 2006; Laurent, Forge et al. 2008; Scarberry, Dickerson et al. 2008; Nel, Maedler et al. 2009; Dykman and Khlebtsov 2012; Elsaesser and Howard 2012; Hellebust and Richards-Kortum 2012; Kanwar, Sun et al. 2012).

According to Chittimalla et al., gold nanoparticles conjugated with DNA can be applied in nucleic acid-based therapies for the delivery of genes to target tumor cells after the nanocomplex is injected into the blood circulation (Chittimalla, Zammuto-Italiano et al. 2005). Moreover, Sato

---

**Electronic supplementary material** The online version of this article (doi:10.1007/s10544-014-9911-z) contains supplementary material, which is available to authorized users.

---

T. Rolim · J. Cancino (✉) · V. Zucolotto  
Nanomedicine and Nanotoxicology Group, Physics Institute of São Carlos, University of São Paulo, CP 369, 13560-970 São Carlos, SP, Brazil  
e-mail: jcancino@ursa.ifsc.usp.br

J. Cancino  
e-mail: jucancino@yahoo.com.br

et al. showed that these nanocomplexes can also be applied in advanced diagnostic systems for the detection of a single base mismatch by using temperature control during the process of nanoparticle aggregation (Sato, Hosokawa et al. 2003). These strategies have also been considered attractive for development of molecular diagnostics devices, capable of determining genetic predisposition to pathologies (Davis, Zuckerman et al. 2010). Despite their extensive application in several research fields, molecular diagnostics are expensive and often inaccessible (Nohaile and Dechairo 2009). There is still a need to develop new low-cost platforms with better efficiency and specificity.

Genosensors based on electrochemical detection show promise in this area. These analytical devices may exhibit low-cost, high specificity and sensitivity, and can be applied for the early detection of genetic diseases (Kerman, Kobayashi et al. 2004; Sassolas, Leca-Bouvier et al. 2008). Bonanni et al. reported the detection of the DNA polymorphism correlated to cystic fibrosis in screen-printed carbon electrodes using an electrochemical device (Bonanni, Isabel Pividori et al. 2009). In a recent study, Civit et al. showed the simultaneous detection of multiple human papillomavirus (HPV) DNA sequences, in which the sensors demonstrated high detection efficiency (Civit, Fragozo et al. 2012).

To obtain the highest possible efficiency using DNA devices, an important factor to be considered is the orientation of the molecules immobilized on the electrode. It has been demonstrated, for example, that orientation of DNA may be achieved upon using mixed self-assembled monolayers (SAM<sub>mix</sub>) (Gebala and Schuhmann 2010). The self-organization between the DNA molecules and the mixed surface that is promoted by the SAM<sub>mix</sub> permits removal of the DNA strands that are adsorbed nonspecifically, resulting in an interface with well-oriented molecules (Schwartz 2001; Mendes, Carvalhal et al. 2008; Gebala and Schuhmann 2010; Campuzano, Kuralay et al. 2011; Cancino and Machado 2012).

Systemic Arterial Hypertension (Mukhtar and Jackson 2013) (SAH) is a disease characterized by the persistence of blood pressure values above the defined normal range. SAH is an independent risk factor for many other diseases. In fact, blood hypertension is considered to be a syndrome that promotes hemodynamic alterations, trophic and metabolic disorders, dyslipidemia, insulin resistance, microalbuminuria, and the deregulation of coagulation factors (Katsi, Marketou et al. 2012; Mukhtar and Jackson 2013). Moreover, SAH is intimately related to several heart diseases such as coronary, cerebrovascular, renal and vascular diseases. Some studies have indicated that approximately 30 % of the world's population may present with this disease by 2025 (Boing and Boing 2007).

Here, we report an electrochemical genosensor that combines the attractive properties of nanomaterials with the

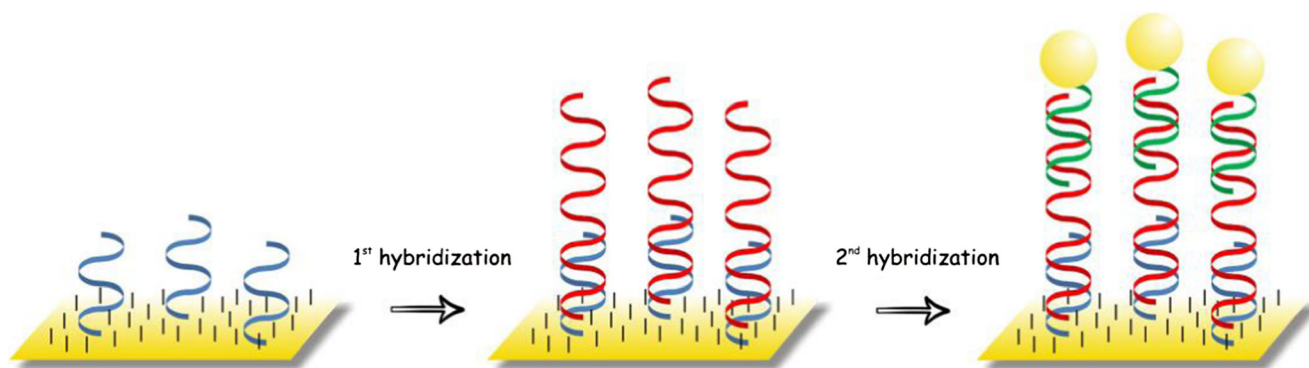
organization features exhibited by SAM<sub>mix</sub> platforms as an innovative approach that shows considerable promise for diagnosis. The key goal of our studies was the fabrication of a genosensor device capable of detecting a specific DNA sequence related to a SAH polymorphism that is located in intron 16 of the ACE gene, which codes for the angiotensin I converting enzyme on locus 17q23. The devices were assembled via the combination of a mixed self-assembled monolayer (SAM<sub>mix</sub>) and a sandwich architecture comprising a capture probe, the target DNA and a report probe DNA conjugated with gold nanoparticles (Scheme 1). We have analyzed and compared two different methods for immobilization of the mixed self-assembled monolayers by monitoring the electrochemical impedance response. Additionally, we have synthesized and characterized a nanocomplex formed by conjugating a DNA report probe with the gold nanoparticles (AuNP-DNA nanocomplexes) used in the genosensing steps. To the best of our knowledge, genosensor devices for Systemic Arterial Hypertension diseases have not been reported in the literature.

## 2 Experimental section

**Materials** Gold chloride solution, polyamidoamine (PAMAM) generation 4 dendrimer, 2-mercaptoethanol, HSCH<sub>2</sub>CH<sub>2</sub>OH (ME), trizma hydrochloride (Tris-HCl), ethylene diamine tetra-acetic acid (EDTA), sodium phosphate monobasic, sodium phosphate dibasic, ethidium bromide solution, potassium hexacyanoferrate (III) (K<sub>3</sub>[Fe(CN)<sub>6</sub>]), acetone solution, ethanol solution, potassium hydroxide and formic acid solution were purchased from Sigma-Aldrich (Brazil) and used without purification. Ultrapure water (18.2 MΩ cm) produced using a Millipore Milli-Q system was used to prepare all aqueous solutions. All oligonucleotides were synthesized by Invitrogen (Life Technologies), and identified as capture, target and report probes. Their sequences are listed in Table S1 in the [supporting information](#).

### 2.1 Instrumentation

*i) Gold nanoparticle and AuNP-DNA nanocomplexes synthesis* A Corning PC-410 magnetic stirrer was used for gold nanoparticle synthesis and for the conjugation of these nanoparticles with oligonucleotides modified for the detection of the SAH polymorphism. The UV-vis absorption spectra of gold nanoparticles and nanocomplexes were measured using a Hitachi U-2900 spectrophotometer. Fourier Transform Infrared Spectroscopy (FTIR) measurements were performed on silicon wafers with a Nicolet 6700 FT-IR from TQ Analyst equipped with an MCT detector and OMINC software. The spectra (4000–400 cm<sup>-1</sup>) were collected from 200



**Scheme 1** Scheme of hybridization in a sandwich format comprising the capture probes (before first hybridization), DNA target probes (after first hybridization), and reporter probes functionalized with gold nanoparticles (AuNP-DNA nanocomplexes) (after second hybridization)

transmission scans with  $4 \text{ cm}^{-1}$  resolution. There were no corrections applied to the spectra, and they were analyzed using GRAMS/AI 7.00 software (©Thermo Galactic). The dynamic light scattering (DLS) and Zeta Potential ( $\zeta$ ) experiments were conducted using a Zetatrac from Microtrac Inc., using 3 scans that were 180 s long for both measurements. Statistical analyses of the size of the gold nanoparticles were performed using Image J software, a public domain software developed by the National Institutes of Health, NIH, USA. *ii) Electrochemical measurements:* Electrochemical measurements were carried out during the detection step by using six gold electrodes (Au electrodes) that had a geometric area of  $0.03 \text{ cm}^2$ . A Pt foil ( $2 \text{ cm}^2$  geometric area) and Ag/AgCl (saturated with  $3 \text{ mol L}^{-1}$  KCl) electrode were used as auxiliary and reference electrodes, respectively, and were employed in all experiments in a conventional borosilicate three-electrode one-compartment electrochemical cell with a PTFE cover. Electrochemical experiments were performed using a PGSTAT40 Autolab electrochemical system (Eco Chemie, Utrecht, Netherlands) equipped with PGSTAT-12 and GPES / FRA 4.9 software (Eco Chemie, Utrecht, Netherlands). Electrochemical impedance spectroscopy (EIS) measurements was carried out in  $0.1 \text{ M}$  PBS (containing  $150 \text{ mol L}^{-1}$  NaCl) buffer solution, pH 7.4, that contained  $5 \text{ mM}$  potassium hexacyanoferrate (III) ( $\text{K}_3[\text{Fe}(\text{CN})_6]$ ) under a frequency range of  $10 \text{ KHz}$  to  $0.1 \text{ Hz}$  with an amplitude of  $0.01 \text{ V}$ . The EIS spectra were represented as Nyquist plots ( $-Z_{\text{im}}$  vs.  $Z_{\text{re}}$ ). *iii) Confocal microscopy:* The images of the genosensor assembly were obtained using a confocal microscope from Nikon Instruments Inc. Images were taken using ethidium bromide (EB), which intercalates with nitrogenous DNA bases, as the fluorescent probe.

## 2.2 Procedures

*i) Gold nanoparticle synthesis* Gold nanoparticles were obtained by the precipitation method, which consisted of the addition of  $1.0 \text{ mmol L}^{-1}$  gold chloride ( $\text{HAuCl}_4$ ) and formic acid ( $\text{CH}_2\text{O}_2$ ) solutions ( $10 \text{ \% v/v}$ ) to a  $0.7 \text{ mmol L}^{-1}$

PAMAM-NH<sub>2</sub> aqueous solution under constant agitation. *ii) Synthesis of Report AuNP-DNA nanocomplexes:* An aliquot of  $1.5 \text{ mL}$  of gold nanoparticles was rinsed twice with ultrapure water to remove any residual PAMAM-NH<sub>2</sub> followed by re-suspension in  $700 \text{ }\mu\text{L}$  of ultrapure water. The complexation started by adding an oligonucleotide solution of the report probe ( $5.8 \text{ pmol}/\mu\text{L}$ ), which was eluted with  $1\text{X TE}$  buffer (containing  $10 \text{ mM Tris-HCl}$  and  $0.1 \text{ mM EDTA}$ ). The complexation solution was kept under constant agitation at  $4 \text{ }^\circ\text{C}$  overnight. *iii) Preparation of SAM<sub>mix</sub> on gold surface electrodes:* The gold electrodes were cleaned being placed in an aqueous solution with  $66 \text{ \% H}_2\text{O}_2$  and concentrated acetone ( $2:1 \text{ v/v}$ ). The electrodes were washed in ultrapure water and ultrasonicated in an ethanol solution for  $10 \text{ min}$  to remove impurities. Afterwards, they were dried using compressed nitrogen gas. The surface modification of the Au electrodes with the SAM<sub>mix</sub> was performed by immersing the electrodes in a mixture of  $0.12 \text{ mM}$  2-mercaptoethanol and  $2 \text{ }\mu\text{M}$  capture probe overnight. The electrodes were washed in ultrapure water to remove non-adsorbed molecules and then used in the electrochemical experiments. Three electrodes were produced for each modification, which had been analyzed by electrochemical impedance spectroscopy during all steps of the modification process using  $\text{K}_3[\text{Fe}(\text{CN})_6]$  as a probe. *iv) Hybridization with target and report AuNP-DNA nanocomplex probes:* The genosensor interface was constructed using a SAM<sub>mix</sub> containing a thiolated capture probe DNA and a spacer thiol, 2-mercaptoethanol. The DNA target was detected by hybridization using a sandwich format composed of the capture and DNA target probes and a reporter probe functionalized with gold nanoparticles (Scheme 1). The hybridization process occurred in two steps. The first hybridization was conducted by immersion of the SAM<sub>mix</sub>-modified electrodes in a  $0.26 \text{ nM}$  oligonucleotide solution of the target probe that was heated to  $54 \text{ }^\circ\text{C}$  for  $10 \text{ min}$ . The electrodes were then cooled to room temperature and rinsed with PBS buffer to remove the excess of non-adsorbed molecules. After the first hybridization, the electrodes were submitted to a second hybridization with nanocomplexes (AuNP-DNA

nanocomplexes) and heated to 54 °C for 10 min. Afterwards, the electrodes were again cooled to room temperature and rinsed with PBS buffer. The hybridization processes were monitored by electrochemical impedance spectroscopy. Confocal microscopy imaging of the electrodes was used to characterize the distribution of the molecules at the Au surface.

### 3 Results and discussion

#### 3.1 Characterization of the report AuNP-DNA nanocomplexes

From the DLS analysis (Fig S1 in Supporting Information), it was determined that the average diameter of the gold nanoparticles without functionalization was approximately 11.0 nm with an average deviation of  $\pm 0.5$  nm. This size was also estimated using the transmission electron microscopy (TEM) images of the nanocomplexes (Fig S2 in Supporting Information). Statistical analysis of the TEM images was conducted using 100 particles, and the average particle size measurement was 11.0 nm with an average deviation of  $\pm 0.43$  nm. The nanoparticles exhibited a zeta potential of +160.3 mV, which was attributed to the presence of protonated amino groups from PAMAM-NH<sub>2</sub> dendrimer used in the synthesis. In contrast, the DLS analysis of the AuNP-DNA nanocomplexes (Fig S3 in Supporting Information) showed an average size of 18.4 nm with an average deviation of  $\pm 0.9$  nm. This distribution was expected because of the 25 bases in the DNA sequence complexed with the gold nanoparticles. Synthetic DNA has a slight twist featuring the Z shape (Rich and Zhang 2003), which decreases the space between the turns and the DNA bases. It is expected that the combination of DNA, which has a negative surface charge, with the PAMAM-NH<sub>2</sub> dendrimer would decrease the zeta potential of the nanocomplexes. The latter was confirmed by zeta potential measurements, revealing a decrease in the potential values from 160.3 to 51.2 mV. However, even with this large reduction, the nanocomplexes remained stable because potentials above 40 mV add to the stability of these compounds (Doane, Chuang et al. 2012).

UV-vis spectra were collected during different steps of the complexation process, as shown in Fig. 1.

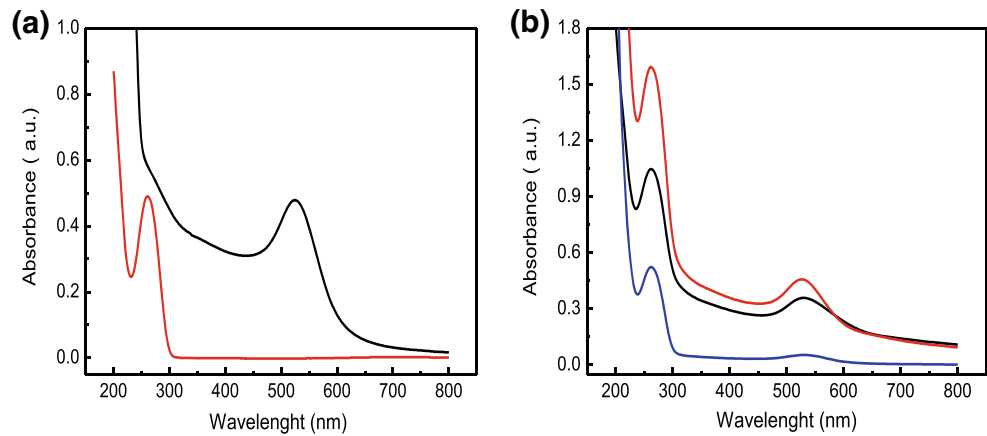
The absorption spectra of the gold nanoparticles were associated with the plasmon band, which depends on the size and shape of the nanoparticles (Wang 2005; Orendorff, Sau et al. 2006; Gao and Tang 2011; Panchapakesan, Book-Newell et al. 2011). Colloidal Au nanospheres (3–100 nm) have an absorbance in the range of 510–570 nm (Liu, Atwater et al. 2007). Figure 1 depicts the UV-vis spectra of the gold nanoparticles with the absorbance peak at 524 nm. Nucleic acids, DNA and RNA exhibit a strong absorbance in the

region between 240 and 275 nm, due to the pyrimidine and purine rings of the nitrogenous bases (Schmid 2001). The UV-vis spectrum of the DNA (Fig. 1a) showed an absorbance at 260 nm. The solution spectrum from Fig. 1b exhibited the absorbance of the gold nanoparticles at 531 nm and the DNA at 260 nm. After centrifugation, the pellet spectrum continued to exhibit the bands of the nanoparticles (531 nm) and the DNA (260 nm), which was an indication that the DNA was conjugated with the nanoparticles. In this case, DNA molecules are too small and lightweight to precipitate alone. Additionally, the absorption band from gold nanoparticles was shifted from 524 to 532 nm upon complexation with the DNA (Fig. 1b), which is evidence of complexation. Moreover, the supernatant spectrum (Fig. 1b) showed lower absorption intensities compared to the re-suspended pellet spectrum, indicating that an excess of DNA was used for complexation.

To investigate the interactions occurring between DNA and the AuNPs, FTIR spectra were collected from gold nanoparticles without functionalization, pure DNA and AuNP-DNA conjugates. The spectra are shown in Fig. 2. In the spectrum of the gold nanoparticles, the band at 3273 cm<sup>-1</sup> corresponds to symmetrical and asymmetrical stretching from NH<sub>2</sub> groups from the PAMAM stabilizing layer. The bands at 1565 cm<sup>-1</sup>, 1652 cm<sup>-1</sup>, are assigned to doublet C = O stretching and deformation N-H/stretch C-N in amides of the interior of PAMAM (Colthup, Daly et al. 1990). The band at 1630 cm<sup>-1</sup> that appears in the DNA spectrum is associated with amine groups (Colthup, Daly et al. 1990; Mady, Mohammed et al. 2011) present in the nitrogenous DNA bases. The bands at 1059 and 1038 cm<sup>-1</sup> are typically assigned to the vibration of ribose (C-C sugar) (Mady, Mohammed et al. 2011) or associated with sulphite groups (Colthup, Daly et al. 1990) which were found in modified phosphate groups in the DNA (-S = P). The band at 1223 cm<sup>-1</sup> is related to the antisymmetric stretching vibration of the phosphate groups (PO<sup>2-</sup>) (Mady, Mohammed et al. 2011). The band at 1065 cm<sup>-1</sup> in the nanocomplex spectrum, which is probably related to the combination of bands at 1059 and 1038 cm<sup>-1</sup> from DNA, appears broader in the nanocomplex, which is indicative that interactions between DNA and AuNPs occurred (Colthup, Daly et al. 1990; Mady, Mohammed et al. 2011). Another indicative of the interactions between DNA and AuNPs comes from the antisymmetric vibration of PO<sup>2-</sup> (1223 cm<sup>-1</sup>) from pure DNA, which changed in both position and intensity after DNA complexation (1231 cm<sup>-1</sup>).

Real-time polymerase chain reaction (PCR) is a technique often used to amplify DNA using a DNA polymerase and fluorescent probes in real-time (Estalilla, Medeiros et al. 2000; Xiang, Benson et al. 2001; Chen, Pan et al. 2011). It has been reported that a combination of capillary sequencing and real-time PCR using gold nanoparticles identified several DNA variations in significant regions of human genomic DNA that are associated with age-related diseases (Chen,

**Fig. 1** **a** UV–vis spectroscopy of gold nanoparticles and DNA. Gold nanoparticles without functionalization (*black line*). Pure DNA spectrum (*red line*). **b** UV–vis spectroscopy after complexation of AuNPs and DNA. Solution spectrum (*red line*), re-suspended pellet spectrum with the AuNP-DNA nanocomplex (*black line*), and supernatant spectrum (*blue line*)



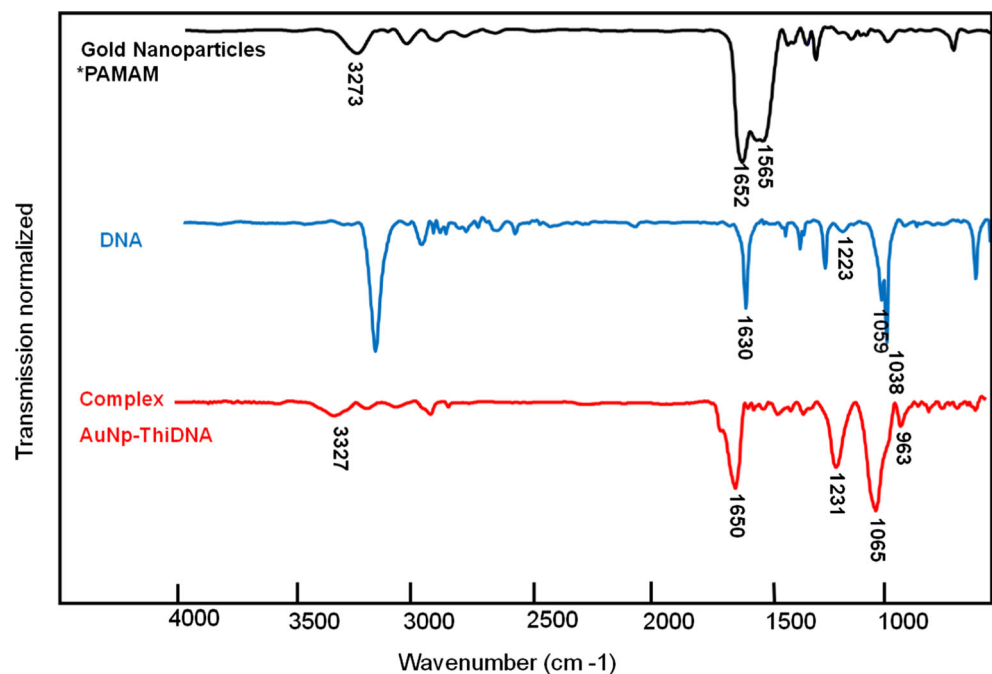
Pan et al. 2011). To investigate the extent of a specific conjugation process between the gold nanoparticles and DNA, the nanocomplexes were submitted to real-time PCR, which was performed with control primers and AuNP-DNA nanocomplexes. The amplification cycles can be found in Fig S4 in the supporting information. The fluorescence spectrum correlates the amplification cycles with the fluorescence units produced during the amplification of template DNA. The SYBR curve (black line) is a baseline factor used in the fluorescent reaction. The intersection of the spectra with the baseline indicates that the amplification reaction of the template DNA has started. The amplification cycles revealed that, at a concentration of  $0.30 \mu\text{M}$ , the nanocomplexes were more efficient to induce amplification than the control primers. The reaction with nanocomplexes (red line) started at cycle 25.6, while

the control primers started the amplification at cycles 27.7 (gray line) and 29.5 (blue line). The analyses were performed using the CFX Manager™ software from BIO-RAD.

### 3.2 DNA detection via electrochemical impedance spectroscopy (EIS)

Electrochemical impedance spectroscopy (EIS) has been used to monitor genosensor devices using the electron transfer resistance ( $R_{ct}$ ) that takes place during the DNA hybridization (Lisdat and Schaefer 2008). This detection is only possible because the molecule that forms a film on top of the surface electrode modulates the electrochemical environment of the interface, which can be detected in the form of changes in the capacitances or

**Fig. 2** FTIR spectra of pure DNA, gold nanoparticles without functionalization and AuNP-DNA nanocomplexes in a transmission standard. The spectra ( $4000\text{--}400 \text{ cm}^{-1}$ ) were collected without applying corrections to the spectra from 200 transmission scans with  $4 \text{ cm}^{-1}$  resolution and analyzed using the software GRAMS/AI 7.00 (©Thermo Galactic)



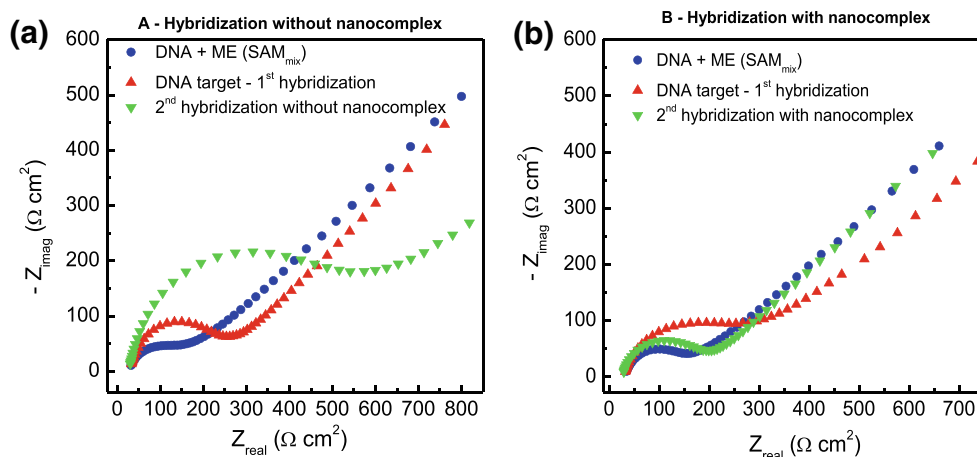


**Fig. 3** Nyquist plots from the modified electrodes during the hybridization processes using target and nanocomplex probes. In both cases, *red symbols* are the signal from the capture DNA + ME-modified electrode. The first hybridization of the target DNA on the modified electrode is represented by *blue symbols*. The last step (*green symbols*)

the charge-transfer rates (Chang and Park 2010). Moreover, electrostatic interfacial repulsion and steric hindrance between charged free-diffusing redox species and the charges of the DNA phosphate backbone were able to change the electrode interface and consequently change the resistances and capacitance during detection (Bonanni, Isabel Pividori et al. 2009; Gebala, Stoica et al. 2009).

The Nyquist plots at each step of the genosensor are shown in Fig. 3 and were obtained during the hybridization processes using target and nanocomplex probes. The EIS measurements were carried out at 0.40 V using an AC perturbation voltage of 0.01 V in the frequency range from 0.1 Hz to 10 kHz in a buffer solution (PBS, pH 7.4) containing 5 mM  $[\text{Fe}(\text{CN})_6]^{3-/4-}$ . Significant differences occurred in the electron transfer resistances in the genosensor experiments in the presence or absence of the nanocomplex (AuNPs-DNA), as shown in Fig. 3.

Figures 3a and b reveals that after the first hybridization of the target DNA on the DNA + ME-modified electrode (capture probe) an increase in the  $R_{ct}$  occurred (blue curves in Fig. 3a and b) (Gebala and Schuhmann 2010; Cancino and Machado 2012). The latter was expected since the hybridization promotes the immobilization of more DNA molecules, increasing the blockage imparted by the recognition layer. However, a more significant difference was observed after the hybridization of the report DNA (second hybridization – green line) on the modified electrode. After hybridization of the report probe without AuNPs (Fig. 3a – green line), a significant increase in the  $R_{ct}$  was observed at the high frequency region of impedance plots, implying in a blocking behavior for  $[\text{Fe}(\text{CN})_6]^{3-/4-}$  reaction. In contrast, the hybridization of the report probe containing the AuNPs (Fig. 3b – green line), a decrease in the resistance ( $R_{ct}$ ) was observed, as a result of the

electron transfer facilitated by the presence of the conducting AuNPs.

When the target DNA was immobilized on the capture DNA + ME electrode surface, a second layer was formed, and the negatively charged phosphate groups of the target DNA structure generated electrical repulsion towards the negatively charged redox marker, inhibiting the interfacial charge transfer process and resulting in an increase in  $R_{ct}$ . In this case, the charged phosphate groups of the target DNA structure

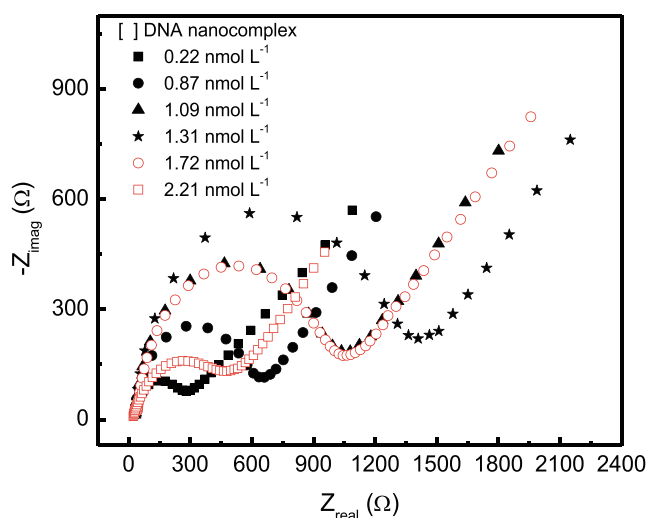


**Fig. 4** Nyquist of the genosensor collected after incubating the electrodes with various AuNP-DNA nanocomplex concentrations (second hybridization). Before each EIS measurement the modified electrode (capture probe) was allowed to interact with the target DNA sequence at a fixed concentration of 0.26 nM. After this first hybridization, the electrodes were subjected to the different concentrations of the AuNP-DNA nanocomplex as indicated in the figure. AC perturbation voltage of 0.01 V in the frequency range from 0.1 Hz to 10 kHz in a buffer solution (PBS, pH 7.4) containing 5 mM  $[\text{Fe}(\text{CN})_6]^{3-/4-}$

overlapped with the positive charges of the protonated hydroxyl groups from the ME SAM<sub>mix</sub> surface, and, consequently, the charge-transfer resistance increased from 142 to 259 Ω - after the first hybridization (Fig. 3a) - and from 159 to 203 Ω (Fig. 3b).

A particular advantage of using the nanocomplexes on the probe was demonstrated in the second hybridization (hybridization of the report probe). After comparing the detection results for the systems with and without the AuNPs-DNA nanocomplex, one may observe that the maximum value of the real part of the impedance,  $Z_{\text{real}}$ , for the nanocomplex probe system in Fig. 3b was 298 Ω, in contrast to the values found for the

genosensor electrode without the AuNPs-DNA nanocomplex (Fig. 3a), which had a charge-transfer resistance  $R_{\text{ct}}$  of 576 Ω.

EIS measurements were carried out using different target DNA concentrations, and the results are shown in terms of electron transfer of  $[\text{Fe}(\text{CN})_6]^{3-/4-}$  according to the amount of target DNA (supporting information Fig S5). The charge transfer resistances after the first hybridization increased as a function of target concentration, revealing that detection of the target DNA is dose-dependent for the range of 1 to 40 nmol L<sup>-1</sup>. The limit of detection for this target DNA detection was calculated to be 0.17 nmol L<sup>-1</sup> with correlation coefficients (R) of 0.9607.

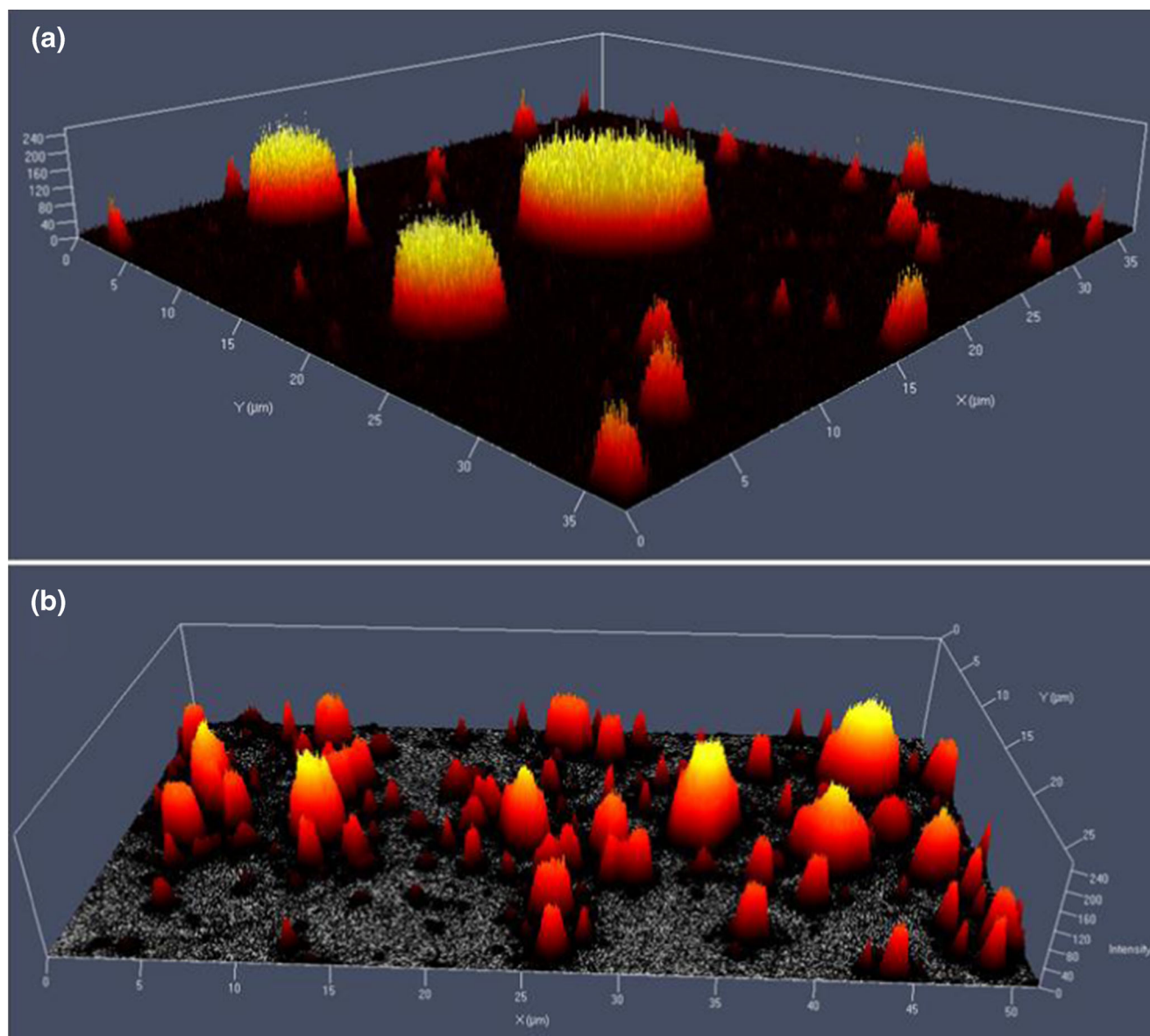


**Fig. 5** 3D confocal images of a gold electrode exposed to ethidium bromide after modification with a SAM<sub>mix</sub> containing the capture probe DNA and 2-mercaptoethanol (ME). The images were acquired after the

first hybridization with the target DNA (a) and after the second hybridization with the AuNP-DNA nanocomplexes (b)

The influence of the amount of DNA-AuNPs report probe on the electrochemical response of the genosensor was also evaluated and a limit of detection of  $0.038 \text{ nmol L}^{-1}$  and correlation coefficient ( $R$ ) of 0.9299 were found. In this case, a DNA + ME modified electrode (capture probe) was allowed to interact with the target DNA sequence – at a fixed concentration of 0.26 nM. After this first hybridization of the target DNA on the electrode, the platform was incubated with different concentrations of the AuNP-DNA nanocomplex (report probe) and the correspondent Nyquist plots appear in Fig. 4.

Two distinct characteristics can be observed for the genosensor containing the AuNP-DNA nanocomplex. In the low concentration range, from 0.22 to 1.31 nM, the electron transfer resistance ( $R_{ct}$ ) increased with increasing concentration of the AuNP-DNA nanocomplex. This was expected because the AuNP concentration is low, and no percolation occurred, meaning that the blocking effect imparted by hybridization surpass the influence of the AuNPs on the conductivity of the system. The AuNP-DNA complex was probably present in a concentration below the percolation threshold. For concentrations of AuNP-DNA nanocomplex above 1.72 nM, the amount of AuNPs in the report probe was sufficient to reduce  $R_{ct}$ , especially for concentrations of 2.21 nM, indicating that electron transfer occurred from the solution to the electrode surface. The latter indicated that for these sandwich-type genosensors based on AuNPs-DNA nanocomplex, performance would be improved when concentrations above 1.7 nM of the report probe is employed.

### 3.3 Confocal imaging of the genosensors platforms

The stepwise building of the genosensor combined with EIS and the observed changes in  $R_{ct}$  represent an efficient strategy for DNA hybridization detection. However, a confirmation of the formation of the complementary DNA sequence is important, especially when two other hybridizations were involved. Confocal microscopy was carried out at each step related to the DNA hybridization detection, using an ethidium bromide marked DNA, as described in the [experimental section](#). The confocal images are shown in Fig. 5.

The confocal image taken after the first hybridization with the target DNA (Fig. 5a) shows that the target DNA is well distributed on the islands formed by the capture DNA probes. After the second hybridization with the AuNP-DNA nanocomplexes (Fig. 5b) the system exhibited a “bowling pins” morphology, corresponding to the sandwich format. Additionally, the second hybridization occurred with a minimum of observed nonspecific interactions compared with the bare

Au surface ([supporting information Fig S6](#)) and the first hybridization.

## 4 Conclusions

We described a sensitive genosensor for Systemic Arterial Hypertension predisposition using the intercalation of suitable DNA and AuNP-DNA nanocomplex probes in combination with EIS. An innovative combination regarding the use of  $\text{SAM}_{\text{mix}}$  –composed by a short ME alkanethiol molecule and the capture DNA probe allowed the formation of island-type morphology that contributed to the charge transfer effects related to the detection method using EIS. Such island structure allowed a better spacing among the DNA probes, facilitating the second hybridization with the target DNA. Successful DNA amplification by control primers and a nanocomplex control were performed using real-time PCR analysis. The EIS results revealed a less inhibition of the redox species and a high sensitivity when the analysis was performed using the AuNP-DNA nanocomplexes. Our strategy represents an efficient method for the unambiguous detection of complementary DNA hybridization for preventative diagnosis of Systemic Arterial Hypertension (SAH).

**Acknowledgments** The authors acknowledge the financial support of the Fundação de Amparo à Pesquisa do Estado de São Paulo - FAPESP (Proc. No. 2010/14565-1), CNPq and CAPES. We are grateful to Dr. Francisco Eduardo Gontijo Guimarães for his help in acquiring the confocal images and Ms. Valéria Spolon Marangoni for TEM images.

## References

- A.C. Boing, A.F. Boing, Hipertensão arterial sistêmica: o que nos dizem os sistemas brasileiros de cadastramentos e informações em saúde. *Rev. Bras. Hipertensão* **14**(2), 84–88 (2007)
- A. Bonanni, M. del Valle, Use of nanomaterials for impedimetric DNA sensors: a review. *Anal. Chim. Acta.* **678**(1), 7–17 (2010)
- A. Bonanni, M. Isabel Pividori et al., Impedimetric detection of double-tagged PCR products using novel amplification procedures based on gold nanoparticles and Protein G. *Analyst* **134**(3), 602–608 (2009)
- S. Campuzano, F. Kuralay et al., Ternary monolayers as DNA recognition interfaces for direct and sensitive electrochemical detection in untreated clinical samples. *Biosens. Bioelectron.* **26**(8), 3577–3583 (2011)
- J. Cancino, S.A.S. Machado, Microelectrodes array in mixed alkanethiol self-assembled monolayers: Electrochemical studies. *Electrochim. Acta* **72**, 108–113 (2012)
- B.-Y. Chang, S.-M. Park, Electrochemical impedance spectroscopy. *Annu. Rev. Anal. Chem.* **3**, 207–229 (2010). E. S. Yeung and R. N. Zare
- P. Chen, D. Pan et al., Gold nanoparticles for high-throughput genotyping of long-range haplotypes. *Nat. Nanotechnol.* **6**(10), 639–644 (2011)
- C. Chittimalla, L. Zammuto-Italiano et al., Monomolecular DNA nanoparticles for intravenous delivery of genes. *J. Am. Chem. Soc.* **127**(32), 11436–11441 (2005)

- L. Civit, A. Frago et al., Electrochemical genosensor array for the simultaneous detection of multiple high-risk human papillomavirus sequences in clinical samples. *Anal. Chim. Acta.* **715**, 93–98 (2012)
- N.B. Colthup, L.H. Daly et al., *Introduction to infrared and Raman spectroscopy* (Academic Press Limited, USA, 1990)
- M.E. Davis, J.E. Zuckerman et al., Evidence of RNAi in humans from systemically administered siRNA via targeted nanoparticles. *Nature* **464**(7291), 1067–U1140 (2010)
- T.L. Doane, C.-H. Chuang et al., Nanoparticle zeta-Potentials. *Acc. Chem. Res.* **45**(3), 317–326 (2012)
- L. Dykman, N. Khlebtsov, Gold nanoparticles in biomedical applications: recent advances and perspectives. *Chem. Soc. Rev.* **41**(6), 2256–2282 (2012)
- A. Elsaesser, C.V. Howard, Toxicology of nanoparticles. *Adv. Drug Deliv. Rev.* **64**(2), 129–137 (2012)
- O.C. Estalilla, L.J. Medeiros et al., 5'→3' exonuclease-based real-time PCR assays for detecting the t(14;18)(q32;21): A survey of 162 malignant lymphomas and reactive specimens. *Mod. Pathol.* **13**(6), 661–666 (2000)
- Y. Gao, Z. Tang, Design and application of inorganic nanoparticle superstructures: current status and future challenges. *Small* **7**(15), 2133–2146 (2011)
- H.M. Garnica-Garza, Contrast-enhanced radiotherapy: feasibility and characteristics of the physical absorbed dose distribution for deep-seated tumors. *Phys. Med. Biol.* **54**(18), 5411 (2009)
- M. Gebala, W. Schuhmann, Controlled orientation of DNA in a binary SAM as a key for the successful determination of DNA hybridization by means of electrochemical impedance spectroscopy. *ChemPhysChem* **11**(13), 2887–2895 (2010)
- M. Gebala, L. Stoica et al., Label-free detection of DNA hybridization in presence of intercalators using electrochemical impedance spectroscopy. *Electroanalysis* **21**(3–5), 325–331 (2009)
- F. Geng, K. Song et al., Thio-glucose bound gold nanoparticles enhance radio-cytotoxic targeting of ovarian cancer. *Nanotechnology* **22**(28), 285101 (2011)
- J.D. Heidel, M.E. Davis, Clinical developments in nanotechnology for cancer therapy. *Pharm. Res.* **28**(2), 187–199 (2011)
- A. Hellebust, R. Richards-Kortum, Advances in molecular imaging: targeted optical contrast agents for cancer diagnostics. *Nanomedicine* **7**(3), 429–445 (2012)
- J.R. Kanwar, X. Sun et al., Nanoparticles in the treatment and diagnosis of neurological disorders: untamed dragon with fire power to heal. *Nanomed. Nanotechnol. Biol. Med.* **8**(4), 399–414 (2012)
- V. Katsi, M. Marketou et al., Impact of arterial hypertension on the eye. *Curr. Hypertens. Rep.* **14**(6), 581–590 (2012)
- L.C. Kennedy, L.R. Bickford et al., A new era for cancer treatment: gold-nanoparticle-mediated thermal therapies. *Small* **7**(2), 169–183 (2011)
- K. Kerman, M. Kobayashi et al., Recent trends in electrochemical DNA biosensor technology. *Meas. Sci. Technol.* **15**(2), R1–R11 (2004)
- S. Laurent, D. Forge et al., Magnetic iron oxide nanoparticles: synthesis, stabilization, vectorization, physicochemical characterizations, and biological applications. *Chem. Rev.* **108**(6), 2064–2110 (2008)
- K.B. Lee, S.J. Park et al., Protein nanoarrays generated by dip-pen nanolithography. *Science* **295**(5560), 1702–1705 (2002)
- F. Lisdat, D. Schaefer, The use of electrochemical impedance spectroscopy for biosensing. *Anal. Bioanal. Chem.* **391**(5), 1555–1567 (2008)
- X. Liu, M. Atwater et al., Extinction coefficient of gold nanoparticles with different sizes and different capping ligands. *Colloids Surf. B Biointerfaces* **58**(1), 3–7 (2007)
- M.M. Mady, W.A. Mohammed et al., Interaction of DNA and polyethylenimine: fourier-transform infrared (FTIR) and differential scanning calorimetry (DSC) studies. *Int. J. Phys. Sci.* **6**(32), 7328–7334 (2011)
- R.K. Mendes, R.F. Carvalho et al., Effects of different self-assembled monolayers on enzyme immobilization procedures in peroxidase-based biosensor development. *J. Electroanal. Chem.* **612**(2), 164–172 (2008)
- O. Mukhtar, S.H.D. Jackson, Risk: benefit of treating high blood pressure in older adults. *Br. J. Clin. Pharmacol.* **75**(1), 36–44 (2013)
- A.E. Nel, L. Maedler et al., Understanding biophysicochemical interactions at the nano-bio interface. *Nat. Mater.* **8**(7), 543–557 (2009)
- M. Nohaile, B. Dechairo, Molecular diagnostics. *Nat. Rev. Drug Discov.* **8**, 337 (2009)
- C.J. Orendorff, T.K. Sau et al., Shape-dependent plasmon-resonant gold nanoparticles. *Small* **2**(5), 636–639 (2006)
- B. Panchapakesan, B. Book-Newell et al., Gold nanoprobe for theranostics. *Nanomedicine* **6**(10), 1787–1811 (2011)
- A. Rich, S.G. Zhang, Z-DNA: the long road to biological function. *Nat. Rev. Genet.* **4**(7), 566–572 (2003)
- A. Sassolas, B.D. Leca-Bouvier et al., DNA biosensors and microarrays. *Chem. Rev.* **108**(1), 109–139 (2008)
- K. Sato, K. Hosokawa et al., Rapid aggregation of gold nanoparticles induced by non-cross-linking DNA hybridization. *J. Am. Chem. Soc.* **125**(27), 8102–8103 (2003)
- K.E. Scarberry, E.B. Dickerson et al., Magnetic nanoparticle-peptide conjugates for *in vitro* and *in vivo* targeting and extraction of cancer cells. *J. Am. Chem. Soc.* **130**(31), 10258–10262 (2008)
- F.-X. Schmid, Biological macromolecules: UV-visible spectrophotometry. *Encyclopedia of life sciences*. (Macmillan Publishers Ltd, Nature Publishing Group, 2001)
- D.K. Schwartz, Mechanisms and kinetics of self-assembled monolayer formation. *Annu. Rev. Phys. Chem.* **52**, 107–137 (2001)
- R. Sinha, G.J. Kim et al., Nanotechnology in cancer therapeutics: bioconjugated nanoparticles for drug delivery. *Mol. Cancer Ther.* **5**(8), 1909–1917 (2006)
- J. Wang, Nanomaterial-based amplified transduction of biomolecular interactions. *Small* **1**(11), 1036–1043 (2005)
- S.D. Xiang, E.M. Benson et al., Tracking membrane and secretory immunoglobulin alpha heavy chain mRNA variation during B-cell differentiation by real-time quantitative polymerase chain reaction. *Immunol. Cell Biol.* **79**(5), 472–481 (2001)